Available online at www.sciencedirect.com
SCIENCE DIRECT
Polymer 45 (2004) 4549–4558
polymer
www.elsevier.com/locate/polymer

A molecular dynamics simulation study of the influence of free surfaces on the morphology of self-associating polymers

Chakravarthy Ayyagari[a], Dmitry Bedrov[b], Grant D. Smith[a,b,*]

[a]*Department of Chemical Engineering, University of Utah, 50 S. Central Campus Dr., Rm. 3290 MEB, Salt Lake City, UT 84112, USA*
[b]*Department of Materials Science and Engineering, University of Utah, 122 S. Central Campus Dr., Rm. 304, Salt Lake City, UT 84112, USA*

Received 4 February 2004; received in revised form 21 April 2004; accepted 22 April 2004

Abstract

Molecular dynamics simulations of thin films and bulk melts of model self-associating polymers have been performed in order to gain understanding of the influence of free surfaces on the morphology of these polymers. The self-associating polymers were represented by a simple bead-necklace model with attractive groups (stickers) at the chain ends (*end-functionalized* polymer) and in the chain interior (*interior-functionalized* polymer). The functionalized groups were found to form clusters in the melt whose size is representative of that found experimentally in many ionomer melts. While the size distribution and shape of the clusters in the thin films were found to be relatively unperturbed compared to their corresponding bulk melts, the morphology of the self-associating melts was found to be significantly perturbed by the free surfaces. Specifically, a strong depletion of stickers near the interface and the emergence of clearly defined layers of stickers parallel to the surface was observed. Increased bridging of clusters by the functionalized polymers was also observed near the free surface. We conclude that these effects can be associated with a high free energy for stickers in the low-density interfacial regime: stickers prefer to be in the higher-density interior of the film where relatively unperturbed sticker clusters can form.

Keywords: Molecular dynamics; Ionomers; Telechelic polymers

1. Introduction

It is well established that the surface morphology and surface properties of a polymer can differ significantly from those of the corresponding bulk polymer [1–3]. In thin polymer films, interfacial effects can in fact dominate the morphology and properties of the polymer [4–7]. The influence of interfaces on polymer morphology is particularly dramatic in block copolymers that undergo self-association, and has been the subject of extensive experimental [8–16], theoretical [17–21] and simulation [22–26] studies.

The surface and thin-film morphology of self-associating random copolymers such as ionomers and thermoplastic elastomers (e.g. polyurethanes) has received significantly less attention. These materials form nanoscopic domains (termed variously clusters, multiplets or micelles) of the minority component (ionomer groups, hard segments, etc.) [27–33] due to preferential self-attraction of these components and/or the desire to minimize interactions between non-compatible groups. These materials are employed in many applications, such as coatings [34,35], proton-exchange membranes [36–38], biomedical implants [39,40] and binders in composites [41,42] where the surface properties of the polymer are paramount. In such materials, it is anticipated that the morphology at the surface may differ significantly from that of the bulk [6]. For example, AFM studies of a poly(ethylene-*co*-methacrylic acid) copolymer film reveal the enrichment of ethylene groups near the surface [43]. While there are several simulation studies of the morphology of self-associating solutions [44–48] and melts [49], to our knowledge there are very few simulation studies [50] of the influence of free surfaces or interfaces on the morphology of these materials.

The primary focus of this work is to gain understanding of the influence of free surfaces on the morphology of self-associating polymers through molecular dynamics (MD) simulations. Specifically, the morphology of bulk melts and thin free-standing films of simple models that represent self-associating polymers are compared. The impact of free

* Corresponding author. Address: Department of Materials Science and Engineering, University of Utah, 122 S. Central Campus Dr., Rm. 304, Salt Lake City, UT 84112, USA. Tel.: +1-801-585-6131; fax: +1-801-581-4816.
E-mail address: gsmith2@cluster2.mse.utah.edu (G.D. Smith).

0032-3861/$ - see front matter © 2004 Elsevier Ltd. All rights reserved.
doi:10.1016/j.polymer.2004.04.044

surface on cluster size and shape, the spatial distribution of clusters, and the interconnectivity of clusters is examined. Additionally, the composition and free energy of the vacuum–polymer interface formed by thin films of self-associating and non-associating polymers are compared. The effect of self-association on capillary waves is also explored.

2. Systems and simulation methodology

MD simulations were performed on the ensemble of 400 chains represented using a bead-necklace model similar to that used in our previous studies of self-associating polymer solutions [44,51]. Each polymer chain was represented as a linear chain consisting of 20 beads with diameter of σ, defining the reference length scale. Bond lengths were constrained at 0.965 using the SHAKE [52] algorithm. All beads interacted via a shifted and truncated (at $r_c = 2.5$) Lennard-Jones potential:

$$U(r) = \begin{cases} U_{LJ}(r) - (r - r_c)\left|\dfrac{dU_{LJ}(r)}{dr}\right|_{r=rc} - |U_{LJ}(r)|_{r=rc}, & r < r_c \\ 0, & r > r_c \end{cases},$$

$$U_{LJ}(r) = 4\varepsilon[(\sigma/r)^{12} - (\sigma/r)^{6}] \quad (1)$$

where $\varepsilon = 1.0$ defining our energy scale. Two beads in each chain are designated as the 'stickers'. In addition to the potential described above, the sticker groups had a short-range attractive potential ($\varepsilon_c = 5.4$) [45]:

$$U_c(r) = -\frac{\varepsilon_c}{r} f(r_c, r),$$

$$f(r_c, r) = \begin{cases} [1 - (r/r_c)^2]^2, & r < r_c \\ 0, & r > r_c \end{cases} \quad (2)$$

Systems with three types of chains have been investigated: (1) no stickers along the chain (reference system); (2) the chain end-groups are stickers (*end-functionalized* polymer), and (3) 6th and 15th atoms in the chain are stickers (*interior-functionalized* polymer). A schematic illustration of these chain structures and the interaction potential between different beads are shown in Fig. 1. For each chain type, film and bulk melt simulations were performed. NPT (constant number of force centers, pressure and temperature) simulations for bulk melt systems were conducted in a 3-dimensional periodic cubic box to determine equilibrium density for these systems at $T^* = 1.33 (T^* = k_B T/\varepsilon)$ and $P^* = 0 (P^* = P\sigma^3/\varepsilon)$. Subsequently, production runs have been performed using an NVT (constant number of force centers, volume and temperature) ensemble and employing an explicit reversible integrator [53]. Film systems were simulated in an orthorhombic periodic box with the film oriented perpendicular to the largest cell dimension (z). The simulation cell size along the z-direction in these systems was chosen large enough to ensure that the film cannot directly interact with its own image. Film systems were simulated using an NVT ensemble. In all systems, a time step of 0.00547 ($t^* = (\varepsilon/m\sigma^2)^{1/2} t$) was used. Initially, the interior-functionalized and reference systems were equilibrated for more than 50 cluster lifetimes (defined below) and then a production run equal to 200 cluster lifetimes was conducted. However, for the end-functionalized systems, equilibration times were less than one cluster lifetime and production runs of one lifetime were utilized due to the very long cluster lifetime in the end-functionalized (see below) systems. As a result, many of the properties discussed below have a significantly larger statistical uncertainty for the end-functionalized systems compared to the reference and interior-functionalized systems.

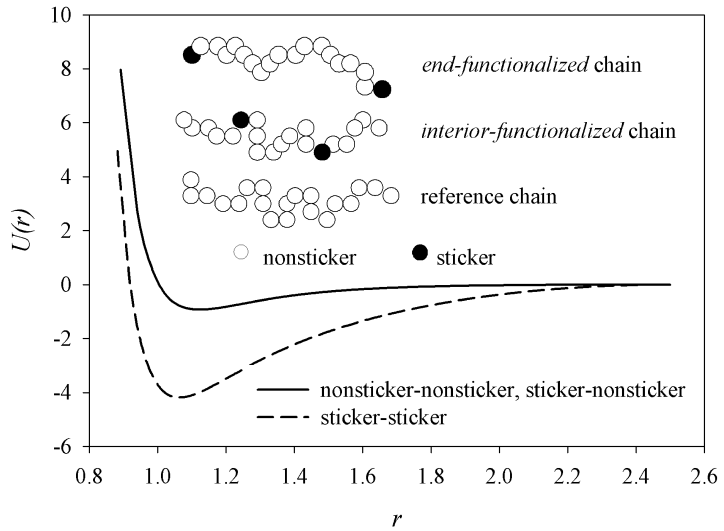

Fig. 1. The sticker–sticker, sticker–nonsticker and nonsticker–nonsticker pair potential as a function of separation distance. Also shown is a schematic illustration of the chain architecture in the reference, interior-functionalized and end-functionalized systems.

Table 1
Average cluster size and mean aspect ratio of clusters in self-associating systems

System	Average cluster size	Aspect ratio		
		R_1	R_2	R_3
Interior-functionalized melt	12.78 ± 0.03[a]	1.51	1.40	1.09
Interior-functionalized film, interior layers	12.69 ± 0.11[b]	1.52	1.41	1.09
Interior-functionalized film, surface layers	12.62 ± 0.07[b]	1.52	1.41	1.09
End-functionalized melt	50.0 ± 6.0[a]	1.60	1.48	1.09
End-functionalized film, interior layers	56.9 ± 5.4[b]	1.57	1.45	1.10
End-functionalized film, surface layers	50.2 ± 5.3[b]	1.54	1.42	1.10

[a] Error bars for melt systems were determined considering the average cluster size sampled over one cluster lifetime as the one statistically independent event and employing a standard error analysis.
[b] Same as in (a) but each layer was considered to be independent from other layers of the same type (surface or interior).

3. Characterization of self-associating polymer melts

The primary focus of this work is to understand the influence of free surfaces on the morphology of self-associating polymers. As the thin free-standing films will be compared to the melts in order to discern the influence of free surfaces on the morphology of self-associating polymers, we begin by analyzing the melt systems. In the functionalized polymer melts the relatively strong attraction between stickers (see Fig. 1) causes them to aggregate into clusters. The clusters are interconnected via chains with stickers belonging to different clusters, resulting in a network of interconnected clusters. We define a sticker as belonging to a particular cluster if it is within a distance of 2.0 from any other sticker in the same cluster. The probability $P(m)$ to find a sticker in a cluster of size m for bulk interior-functionalized melt is shown in Fig. 2. The distribution for the end-functionalized melt is not shown due to relatively large statistical noise. The probability distribution indicates that there is a preferable size cluster $m \approx 13$ in the interior-functionalized melt. This cluster size corresponds well with that observed experimentally in several ionomer melts [54,55] indicating that the interior-functionalized polymer is a reasonable model for cluster formation in ionomer melts where cations and anions remain closely associated. As shown in Table 1, the average cluster size is much larger in the end-functionalized melt compared to the interior-functionalized melt. In the model interior-functionalized melt the attractive groups are hindered in the middle of the chain and hence have more steric constrains to aggregate [27,47,48] compared to the end-functionalized chain, where the attractive groups are located at the chain ends.

The lifetime of well-defined clusters ($m \geqq 5$) in the self-associating melts was estimated by examining the cluster lifetime autocorrelation function, given as

$$C(t) = \frac{\sum_{i \neq j} H_{ij}(t) H_{ij}(0)}{\sum_{i \neq j} H_{ij}(0) H_{ij}(0)} \tag{3}$$

Here, the summation is performed over every pair (i,j) of sticker groups. The function $H_{ij}(t) = 1$ if sticker groups i and j belong to the same cluster at time t, otherwise $H_{ij}(t) = 0$. The sticker lifetime autocorrelation functions for the end-functionalized and interior-functionalized bulk melts are

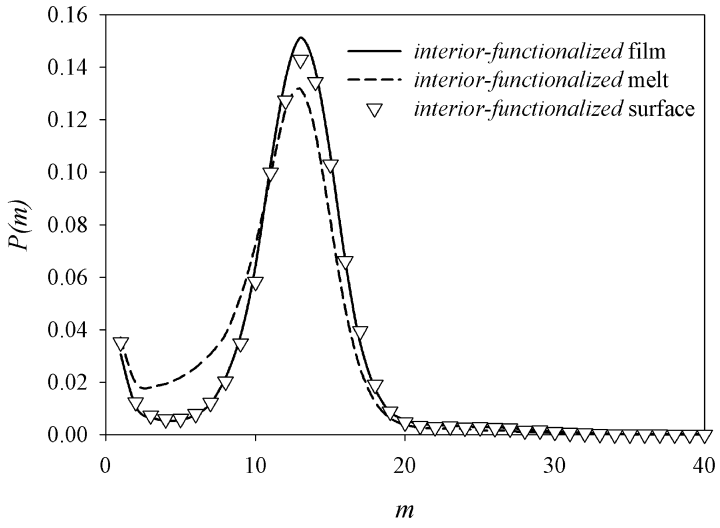

Fig. 2. Cluster size distribution of the interior-functionalized melt and film.

shown in Fig. 3, along with fits of a stretched exponential (KWW)

$$C(t) = \exp(-(t/\tau)^{\beta}) \quad (4)$$

to the autocorrelation functions. The cluster lifetimes, given in Fig. 3, are taken to be the time constants τ from the stretched exponential fits. It can be seen that the cluster lifetime for the end-functionalized melt is significantly longer than that for the interior-functionalized melt, resulting in relatively poor statistics for the former (see Section 2 above).

The spatial correlations between stickers in the melt are revealed in the sticker–sticker pair distributions shown in Fig. 4. The sticker–sticker correlations are quite different for end-functionalized and interior-functionalized melts beyond the first coordination shell ($r > 1.5$). The enhanced structure in the sticker–sticker distribution functions for end-functionalized melt (increased intensity of the second and third peaks) is consistent with ability of the end-functionalized chains to form larger clusters as discussed above. Depletion of stickers in the end-functionalized melt in the interval 4–8σ compared to the interval 3–5σ for the interior-functionalized melt reflects the larger spacing between the clusters along the end-functionalized chains.

The shape of the clusters was determined by examining the ratio of eigenvalues (λ_1, λ_2, λ_3) corresponding to the principal moments of inertia of a cluster ($m \geqq 5$). The aspect ratios are given by $R_1 = (\lambda_3/\lambda_1)^{1/2}$, $R_2 = (\lambda_2/\lambda_1)^{1/2}$, $R_3 = (\lambda_3/\lambda_2)^{1/2}$ where $\lambda_1 \leq \lambda_2 \leq \lambda_3$. The aspect ratios (shown in Table 1) indicate that the clusters are roughly spherical (1 = perfect sphere) in both self-associating melts.

Finally, we examined the connectivity between clusters by determining the fraction of chains participating as tails, bridges, loops and free chains. A tail refers to a chain with one sticker participating in a well-defined cluster ($m \geqq 5$)

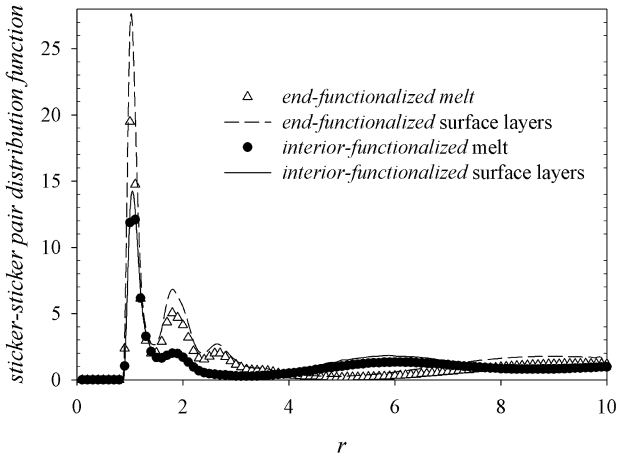

Fig. 4. Sticker–sticker pair distribution function in the self-associating melts. Also shown is the 2-dimensional sticker–sticker distribution function in the surface layers for the self-associating films.

while the other is not associated with any cluster (i.e. it participates in a cluster of size $1 \leq m < 5$). A bridge is formed between clusters if the two stickers in a chain are associated with two different clusters (each with $m \geqq 5$). A free chain does not have any association with a cluster of $m \geqq 5$ and a loop is formed if both the stickers in a chain belong to the same cluster ($m \geqq 5$). The average fractions of tails, loops, bridges and free chains for the self-associating melts are reported in Table 2. For both the end-functionalized and interior-functionalized melts the fraction of free chains is negligible. In the end-functionalized melt we observe a larger fraction of chains participating in bridges due to the greater distance between stickers along a chain (see Fig. 1), which facilitates formation of bridges [49]. The number of bridges between any two participating clusters (averaged over all cluster pairs with at least one bridge), the number of loops in a cluster (averaged over clusters with at least one loop), the number of tails emerging from a cluster

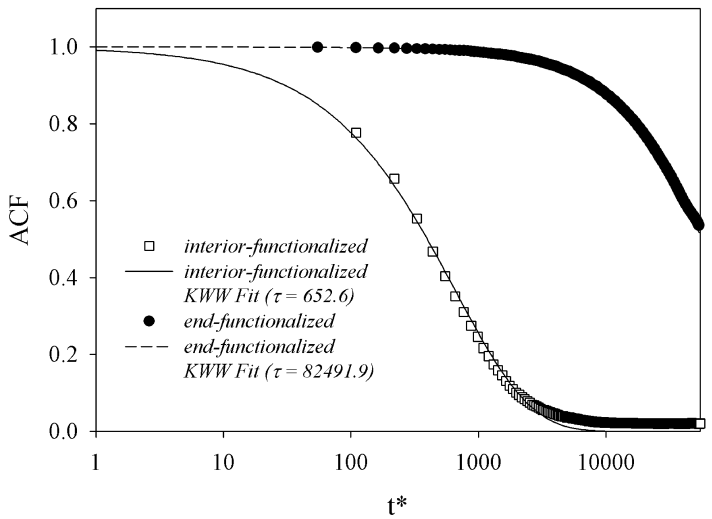

Fig. 3. Cluster lifetime autocorrelation function for interior-functionalized and end-functionalized melts. Also shown are the corresponding fits to stretched exponential function (KWW) and cluster lifetimes.

(averaged over clusters with at least one tail emerging) is also given for the self-associating melts in Table 2. The end-functionalized melt, which more easily forms bridges and has bigger clusters, exhibits significantly more bridges between the clusters than observed in the interior-functionalized melt.

4. Characterization of self-associating polymer films

4.1. Film density profiles

We begin our analysis of the morphology of the free standing end-functionalized and interior-functionalized films by examining the overall bead density profiles. In Fig. 5(A) the density profiles along z-direction (perpendicular to the film surfaces) for the self-associating and reference (non-associating) films are compared. Also shown are the corresponding densities in the bulk melt (straight horizontal lines) for each system. In the self-associating systems, both films and bulk melts, attraction between stickers tends to increase the density compared to the corresponding reference (non-associating) systems. Structure not present in the density profile for the reference film can be seen in the self-associating films and is discussed in detail below.

4.2. Sticker and end-group density profiles

The density profiles of stickers only for the self-associating films are shown in Fig. 5(B). The free surface induces ordering of stickers perpendicular to the surface. The layering is sharp near the free surfaces and gradually decreases as one moves away from the interface. The thickness of the films considered in this work is not sufficient to observe the melt-like (no preferred layering) structure at the center of the films. The clusters are larger in the end-functionalized film than in interior-functionalized film, and hence we observe only three, relatively wide layers of stickers in the former while five layers form in the latter

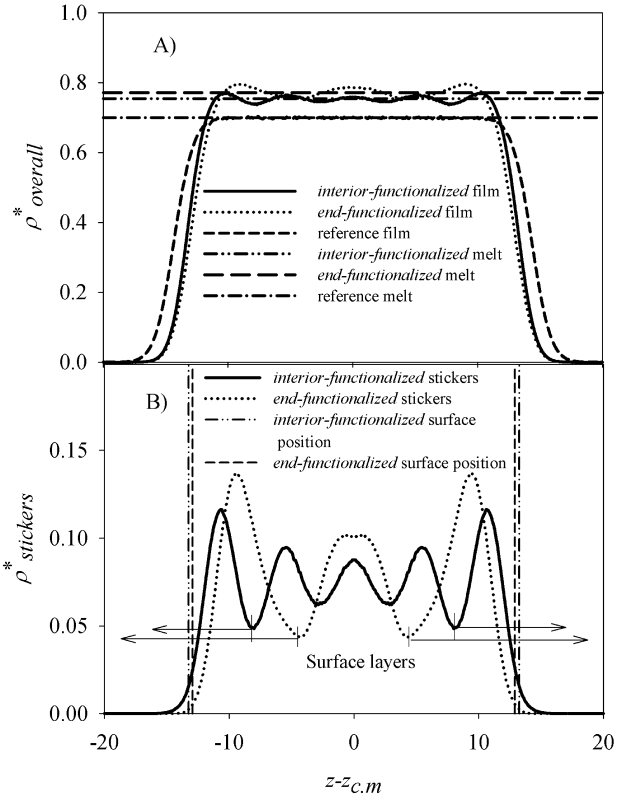

Fig. 5. (A) Density profiles for films as a function of z-coordinate with respect to the center of mass of the film. Straight lines represent melt densities. (B) Density profile of sticker beads in the self-associating films and the definition of layers. The position of the surfaces (see text for definition) is indicated by vertical lines. The surface layers are indicated by horizontal arrows.

film of approximately the same thickness. The dashed vertical lines in Fig. 5(B) indicate the location of the surface obtained by fitting the overall density profile in Fig. 5(A) to the tanh function [50] (position = h in Eq. (5)).

$$\rho(z) = \tfrac{1}{2}\rho_{\text{bulk}}(z)\{1 - \tanh[2(z-h)/w]\} \quad (5)$$

where $\rho(z)$ is the density at position z, $\rho_{\text{bulk}}(z)$ is the bulk density, h is the position of the interface and w is the surface

Table 2
Fraction of bridges, loops, tails and free chains in self-associating systems

System	Bridges	Loops	Tails	Free chains
Interior-functionalized melt	0.65[a] (1.31)[c]	0.26 (2.00)	0.08 (1.03)	0.00 (−)
Interior-functionalized film, interior layers[d]	0.49[a] (1.32)	0.43 (1.97)	0.08 (1.04)	0.00 (−)
Interior-functionalized film, surface layers[b]	0.44[a] (1.43)	0.44 (2.39)	0.11 (1.04)	0.01 (−)
End-functionalized melt	0.79[a] (3.37)	0.21 (5.47)	0.00 (1.00)	0.00 (−)
End-functionalized film, interior layers[a]	0.48[a] (4.16)	0.51 (5.46)	0.00 (1.00)	0.00 (−)
End-functionalized film, surface layers[b]	0.55[a] (4.67)	0.45 (8.67)	0.00 (1.00)	0.00 (−)

[a] All cross-layer bridges are excluded.
[b] Averaged over two surface layers (defined in Fig. 5(B)).
[c] Numbers in parentheses are the average number of bridges between any two clusters, average number of loops in a cluster and average number of tails emerging from any cluster correspondingly).
[d] Averaged over all bulk layers (defined in Fig. 5(B)).

thickness (interfacial width). It can be clearly seen that the stickers are 'buried' below the interface. This behavior can be understood in terms of the free energy penalty of having a sticker group in the less-dense interfacial region, where the bead–bead coordination number is dramatically reduced. Hence, the surface interferes with the ability of the stickers to aggregate and form clusters of optimal size and shape. The attractive sticker–sticker energy drives the stickers away from this region, and results in the formation of a well-defined layer of stickers just below the interface where sticker–sticker contacts can be maintained. The formation of this first 'surface' layer of stickers promotes the formation of a second layer with an intervening region largely occupied by non-associating groups. The surface layer is defined as the region from the first minimum in density of stickers outward from the film, as illustrated by horizontal arrows in Fig. 5(B).

We have also calculated the normalized fraction of end groups and stickers using the following relation:

$$f(z) = \left[\frac{N_i(z)}{N_i}\right]\left[\frac{N}{N(z)}\right] \quad (6)$$

where $N_i(z)$ is the number of beads of type i (i = 'stickers' or 'end-groups') in the slab oriented parallel to the surface and centered at distance z from the film center of mass position, N_i is the total number of beads of type i in the film, $N(z)$ is the total number of any beads in the slab at z and N is the total number of all beads in the film. Fig. 6 shows the fraction profile for sticker and end groups in the reference and self-associating films along the z-direction. The $f(z)$ calculated using Eq. (6) indicates an enrichment ($f(z) > 1$) or depletion ($f(z) < 1$) of stickers or chain ends as a function of position in the film. We observe that in the reference (non-associating) film the chain ends prefer the surface due their relatively low cohesive energy density [50, 56] and the relatively low entropy penalty for having chain ends at an interface [57]. In the case of interior-functionalized chains there is a significant enrichment of chain ends at the surface due to additional structure imposed by the presence of the sticker layer just below the surface and the depletion of stickers at the surface. In the end-functionalized film the chain ends are stickers and hence do not want to populate the surface. The favorable energetics due to aggregation of the stickers (chain ends) in the end-functionalized film below the surface dominates any favorable entropic effect that would be associated with enrichment of chain ends at the surface.

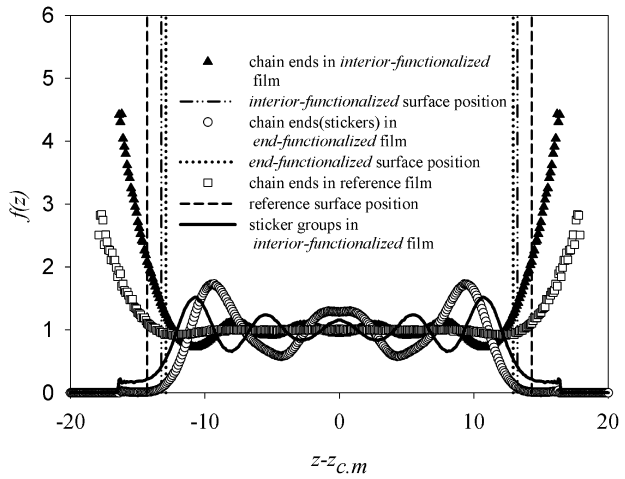

Fig. 6. Normalized fractions (see Eq. (6) in text) of endgroups/stickers in the films as a function of z-coordinate with respect to the center of mass of the film. The position of the surfaces (see text for definition) is also shown.

4.3. Cluster size, shape and sticker–sticker distribution

In order to investigate the effect of the free surface on the size and shape of the sticker clusters, we compared the size distribution of clusters in the interior-functionalized film to that in the corresponding melt in Fig. 2. The cluster size distribution in the film is quite similar to that in the melt. Also shown in Fig. 2 is the size distribution of clusters in the surface layer (see Fig. 5(B) for definition of layers). Stickers form clusters of approximately the same size in the interior film layers, the surface film layers and the bulk melt. Additionally, the clusters maintain their roughly spherical shape in the film, including the surface layer, as revealed in Table 1. Hence, the presence of free surface does not appear to significantly perturb the shape and size of the clusters. Similar observations can be made regarding clusters in the end-functionalized film within statistical uncertainties, as shown in Table 1.

A 2-dimensional sticker–sticker pair distribution function was calculated by dividing the film into sub-layers of thickness 0.5 and observing the distribution of distances between any two stickers within a given sub-layer. The 2-dimensional sticker–sticker pair distribution functions (weighted by the density of pairs and averaged over all

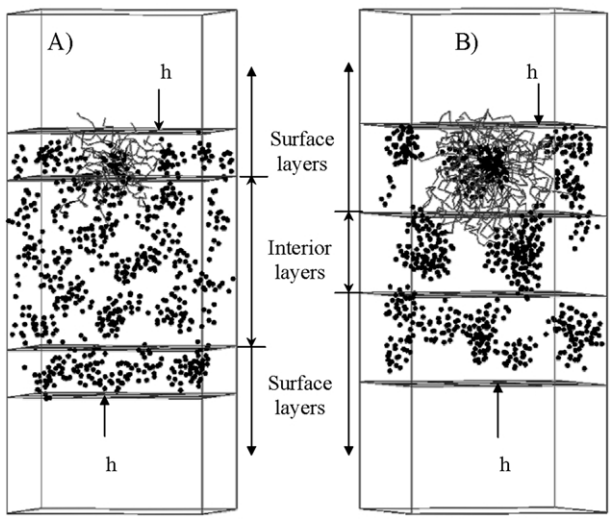

Fig. 7. Snapshot of interior-functionalized (A) and end-functionalized (B) films illustrating clusters (for clarity the nonstickers are shown for one surface cluster only). The position of the surfaces (h in Eq. (5)) and the layers are indicated.

sub-layers) for surface layer are compared to the sticker–sticker pair distribution functions in the melt in Fig. 4 in order to elucidate any influence of the free surface on the lateral structure of the film. We observe that the free surface does not qualitatively influence the spatial distribution of stickers (and hence of sticker clusters) parallel to the surface, in other words, there is no indication of enhanced ordering of sticker groups within the layers. We can therefore conclude that within the layers stickers exist in clusters that closely resemble those found in the bulk melt and that the layering of sticker groups shown in Fig. 5(B) for the self-associating films corresponds to layering of sticker clusters. Fig. 7 illustrates the layering of clusters in the self-associating films. Also shown in Fig. 7 is one surface cluster with all chain units (sticker and non-associating). In contrast to the end-functionalized film the chain ends of the surface clusters in the interior-functionalized film tend to extend outward from the surface layer. The position of the surface (h in Eq. (5)), surface and interior layers for the self-associating films are also illustrated in Fig. 7.

4.4. Cluster interconnectivity

The fraction of bridges, loops, tails and free chains (as defined previously) for self-associating films are shown in Table 2 for the surface layers and interior layers of the films. The values for interior layers are obtained by averaging over all interior layers (non-surface layers) whereas the values for surface are averaged over the two (one on each side of the film) surface layers. The fraction of bridges does not include the bridges between clusters in different layers and hence the fraction of bridges does not correspond to the melt, even for the interior film layers. Despite the neglect of inter-layer bridging we observe that the extent of cluster bridging in the films is greater than that observed in the bulk melts, indicating that layering of the clusters induced by the free surfaces results in increased bridging within layers, particularly in the surface layer.

4.5. Characterization of the free surface

The interfacial width or the surface thickness (w) along with the position of the surface can be obtained by fitting the total density profile of each system to tanh function [50] (see Eq. (5)). The interfacial widths for studied systems are tabulated in Table 3. We further investigated the structure of the surface by analyzing the distribution of lengths of the segments of each chain that are located at the surface. For this purpose the surface is defined as the region of thickness w from $h - w/2$ to $h + w/2$, where h is the position of the surface and w is the interfacial width. Fig. 8 shows a probability (weighted by the length of the segment, N) of finding a segment of N beads at the surface, averaged over both surfaces. The average segment length at the surface determined from distributions in Fig. 8 is 7.4, 8.6, and 8.3 for interior-functionalized, end-functionalized and reference films, respectively. In the case of the interior-functionalized film, there is an enrichment of short segments at the surface. Here the stickers, which prefer to be away from the surface, are in the interior of the chain and thus restrain the maximum length of chain segment that can populate the surface. In the end-functionalized film there is an increased probability of finding much longer chain segments at the surface, consistent with the greater distance (along a chain) between the 'surface-hating' functionalized groups.

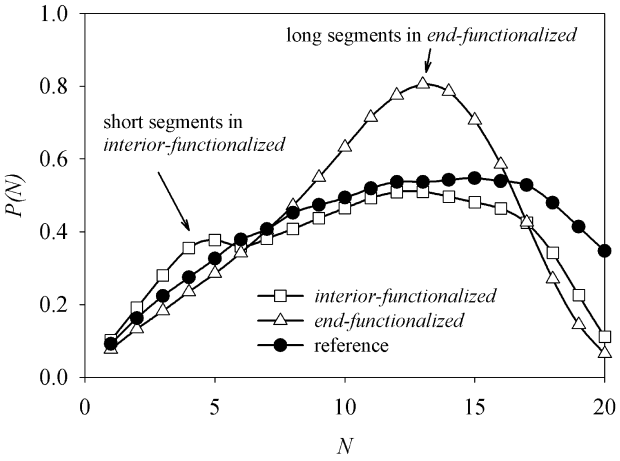

Fig. 8. Probability of segments of length N (weighted by N) at the surface (see text for definition of surface) for the films.

We also analyzed capillary waves [58,59] at the surface in order to understand the influence of self-association on capillary wave formation. The width of the interface, observed from fitting the average density profiles (obtained by averaging the entire film) to tanh functions in Eq. (5), includes the broadening of the width due to capillary waves. The width thus obtained would also include the fluctuations of the surface position itself. These fluctuations determine the roughness of a surface. In order to determine the fluctuations of the interface, it is convenient to split the film into columns perpendicular to the surface (z-direction) and to determine the local interface position, $h(x, y)$ by fitting the

Table 3
Surface tension, average thickness and surface width of simulated thin films

System	Surface tension (γ^*)	Average thickness (L_z)	Surface thickness or interfacial width (w)
Interior-functionalized	0.088 ± 0.008	26.51	2.52
End-functionalized	0.121 ± 0.009	25.83	2.86
Reference	0.081 ± 0.003	28.62	2.95

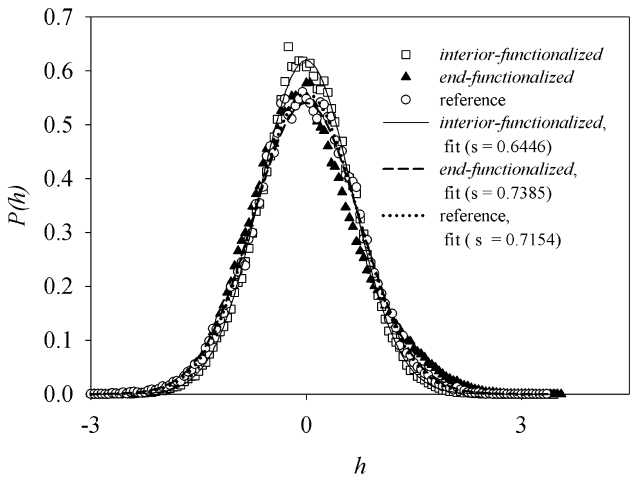

Fig. 9. Distribution of local interface position (for columns of size $B \times B \times L$, $B = 6.66\sigma$, $L = L_z$) and their corresponding Gaussian fits (s = width of the Gaussian). See Eq. (7) in text.

density profiles to tanh function (Eq. (5)) in each column individually. We have divided the simulation box into nine columns ($B \times B \times L_z$), where $B = 6.66\sigma$ and L_z is the thickness of the film. The value of B approximately corresponds to the theoretical predictions of coarse graining length scale [58]. The distributions of the local interface position for the films are shown in Fig. 9. The width of these distribution (s) can be obtained by fitting to a Gaussian function given below in Eq. (7) and is directly related to the smoothness of the surface (smaller s and therefore narrower distribution corresponds to a smoother surface) [60]

$$P(h) = \frac{1}{\sqrt{2\pi s^2}} \exp\left(-\frac{h^2}{2s^2}\right) \tag{7}$$

Distribution widths indicate that the surface of the interior-functionalized film is the smoothest while that of the end-functionalized film is the roughest. It is interesting that the extent of surface roughness correlates nicely with the average segment length at the surface discussed above. In the interior-functionalized film layering of clusters along the surface and the propensity for the surface to be populated by chain ends results in a higher probability to find relatively short chain segments at the surface. This, in turn, can effectively limit density fluctuations at the surface, as these relatively short segments tend to be 'tied' into the layer of sticker clusters just below the surface. In the end-functionalized film, where the length of chain segments populating the surface is larger than in the interior-functionalized film, the distribution width of interfacial position is the broadest and hence the surface in this system has the largest roughness. It is reasonable to suggest that the longer chain segments populating the surface in the end-functionalized film perhaps are more suited to support larger density fluctuations than the shorter segments in interior-functionalized film. The difference between the surface roughness in the end-functionalized and interior-functionalized films indicate that the self-association and layering of sticker clusters alone are not enough to reduce the surface roughness. The chain architecture (position of sticker groups in the chain and length of the chain) and its influence on the intercluster structure are the key factors controlling the surface roughness. Our simulations indicate that the capillary waves that can cause solid substrate dewetting [61, 62] or lead to mechanical instability of the film can be suppressed or controlled by choosing an optimal chain architecture for a given underlying structure of the self-assembled polymer film.

Finally, we calculate the interfacial (surface tension) for the films using the relation [63–65]

$$\gamma = [P_{zz} - 1/2(P_{xx} + P_{yy})] \times L_z \tag{8}$$

where P_{xx}, P_{yy} and P_{zz} are the components of pressure tensor and L_z is the thickness of the film. The average thickness of the film is obtained by fitting the total density profile to tanh function ($L_z = 2\,h$, h is the position of the interface as given by Eq. (5). The surface tension in reduced units ($\gamma^* = \gamma\sigma^2/\varepsilon$) for the films are tabulated in Table 3. The surface tensions of the reference and interior-functionalized films are comparable, indicating that the interfacial free energy contribution due to the frustration of cluster formation by the free surface is minimal for the interior-functionalized film. It may be that unfavorable entropic effects associated with the layering of the clusters in the interior-functionalized film are largely offset by the enrichment of chain ends at the surface, at least for the low-molecular weight chains investigated here. For the end-functionalized film a significant increase in interfacial tension is observed compared to the reference film, consistent with the stronger layering and inability of the end-functionalized film to populate the interface with chain ends. It may also be that the relatively larger clusters formed by the end-functionalized chains are more perturbed by the presence of the surface, as evidenced by the increased number of tails and bridges within the first layer (see Table 2), thereby contributing to the interfacial free energy. The statistics on cluster size are not sufficient for the end-functionalized film to determine whether the size of the clusters is quantitatively perturbed (Table 1).

5. Conclusions

The influence of free surfaces on cluster formation in thin films of self-associating polymers has been investigated using MD simulations. Our simulations reveal that free surfaces significantly perturb the morphology of the film perpendicular to the surfaces exhibited by a strong depletion of functionalized groups at the surface and the formation of layers of clusters of functionalized groups below the film surface. This perturbation (layering) persists well into the interior of the film and introduces structure, on the length scale of the mean spacing between clusters, which is

significantly greater than in bulk melts of the self-associating polymers. This 'burying' of functionalized groups below the surface is thought to be due a free energy driving force that restricts self-associating groups from populating the low-density surface and promotes the formation of 'optimal' clusters, i.e. clusters with a size distribution and shape similar to that found in the bulk melt. The influence of free surfaces on the morphology of these self-associating polymers, the dependence upon the surface-induced structure and interfacial properties on the architecture of the polymer, and the persistence of the induced structure well into the interior of the films have important implications for the understanding of interfacial properties of self-associating polymer melts, particular in applications dominated by interfaces such as thin films and polymer nanocomposites.

Acknowledgements

This work was supported by CRC-NSF Grant 0R4649-001.03 (University of Tennessee) and University of Utah Center for Simulations of Accidental Fires and Explosions (C-SAFE) funded by Department of Energy, Lawrence Livermore National Laboratory, under subcontract No. B524196. We would also like to acknowledge the support of NASA Langley Research Center through grant NAG 12319.

References

[1] Sanchez IC. Physics of polymer surfaces and interfaces. Stoneham: Butterworth-Heinemann Manning; 1992.
[2] Chan C-M. Polymer surface modification and characterization. New York: Hanser; 1994.
[3] Karim A, Kumar S. Polymer surfaces, interfaces and thin films. River Edge: World Scientific; 2000.
[4] Zhu J, Eisenberg A, Lennox RB. Macromolecules 1992;25:6547.
[5] Shin K, Pu Y, Rafailovich MH, Sokolov J, Seeck OH, Sinha SK, Tolan M, Kolb R. Macromolecules 2001;34:5620.
[6] Hill TA, Carroll DL, Czerw R, Martin CW, Perahia D. J Polym Sci Part B: Polym Phys 2003;41:149.
[7] Amitay-Sadovsky E, Komvopoulos K, Tian Y, Somorjai GA. Appl Phys Lett 2002;80:1829.
[8] Hong S, MacKnight WJ, Russell TP, Gido SP. Macromolecules 2001; 34:2398.
[9] Rockford L, Mochrie SGJ, Russell TP. Macromolecules 2001;34: 1487.
[10] Jeoung E, Galow TH, Schotter J, Bal M, Ursache A, Tuominen MT, Stafford CM, Russell TP, Rotello VM. Langmuir 2001;17:6396.
[11] Xu T, Goldbach JT, Russell TP. Macromolecules 2003;36:7296.
[12] Russell TP, Anastasiadis SH, Menelle A, Felcher GP, Satija SK. Macromolecules 1991;24:1575.
[13] Shull KR, Winey KI, Thomas EL, Kramer EJ. Macromolecules 1991; 24:2748.
[14] Dai C-A, Kramer EJ, Shull KR. Macromolecules 1992;25:220.
[15] Hashimoto T, Koizumi S, Hasegawa H. Macromolecules 1994;27: 1562.
[16] Bukowski A, Klein J, Fetters LJ, Hashimoto T. Macromolecules 1995; 28:8579.
[17] Matsen W. J Chem Phys 2001;114:10528.
[18] Duque D, Schick M. J Chem Phys 2000;113:5525.
[19] Geisinger T, Müller M, Binder K. J Chem Phys 1999;111:5251.
[20] Nath SK, McCoy JD, Curro JG, Saunders RS. J Chem Phys 1997;106: 1950.
[21] Whitmore MD, Noolandi J. J Chem Phys 1990;93:2946.
[22] Banaszak M, Wołoszczuk S, Jurga S, Pakula T. J Chem Phys 2003; 119:11451.
[23] Schultz AJ, Hall CK, Genzer J. J Chem Phys 2002;117:10329.
[24] Grest GS, Lacasse M-D, Kremer K, Gupta AM. J Chem Phys 1996; 105:10583.
[25] Dotera T, Hatano A. J Chem Phys 1996;105:8413.
[26] Fried H, Binder K. J Chem Phys 1991;94:8349.
[27] Hird B, Eisenberg A. Macromolecules 1992;25:6466.
[28] Gouin J-P, Bosse F, Nguyen D, Williams CE, Eisenberg A. Macromolecules 1993;26:7250.
[29] Gao Z, Eisenberg A. Macromolecules 1993;26:7353.
[30] Nguyen D, Williams CE, Eisenberg A. Macromolecules 1994;27: 5090.
[31] Wang H, Palmer RA, Schoonover JR, Graff DK. AIP Conf Proc 2000; 31.
[32] Graff DK, Wang H, Palmer RA, Schoonover JR. Macromolecules 1999;32:7147.
[33] Chitanvis SM. Phys Rev E 1998;57:1921.
[34] Whiteley LD, Martin CR. Anal Chem 1987;59:1746.
[35] Matysik F-M, Matysik S, Brett AMO, Brett CMA. Anal Chem 1997; 69:1651.
[36] Jiang S, Xia K-Q, Xu G. Macromolecules 2001;34:7783.
[37] Rubatat L, Rollet AL, Gebel G, Diat O. Macromolecules 2002;35: 4050.
[38] Rubinstein I, Bard AJ. J Am Chem Soc 1981;103:5007.
[39] Amitay-Sadovsky E, Komvopoulos K, Ward R, Somorjai GA. J Phys Chem B 2003;107:6377.
[40] Berrocal MJ, Badr IHA, Gao D, Bachas LG. Anal Chem 2001;73: 5328.
[41] Lewis JP, Sewell TD, Evans RB, Voth GA. J Phys Chem B 2000;104: 1009.
[42] Smith GD, Bedrov D, Byutner O, Borodin O, Ayyagari C, Sewell TD. J Phys Chem A 2003;107:7552.
[43] Sauer BB, McLean RS. Macromolecules 2000;33:7939.
[44] Bedrov D, Smith GD, Douglas JF. Europhys Lett 2002;59:384.
[45] Khalatur PG, Khokhlov AR, Mologin DA. J Chem Phys 1998;109: 9614.
[46] Khalatur PG, Khokhlov AR, Kovalenko JN, Mologin DA. J Chem Phys 1999;110:6039.
[47] Kim SH, Jo WH. Macromolecules 2001;34:7210.
[48] Timoshenko EG, Kuznetsov YA. Europhys Lett 2001;53:322.
[49] Sung BJ, Yethiraj A. J Chem Phys 2003;119:6916.
[50] Jang JH, Ozisik R, Mattice WL. Macromolecules 2000;33:7663.
[51] Bedrov D, Smith GD, Douglas JF. Polymer 2004;45(11):3961–6.
[52] Ryckaert J, Ciccotti G, Berendsen HJC. J Comput Phys 1997;23:327.
[53] Martyna GJ, Tuckerman ME, Tobias DJ, Klein ML. Mol Phys 1996; 87:1117.
[54] Eisenberg A, King M. Ion containing polymers. New York: Academic Press; 1977.
[55] Eisenberg A, Kim J-S. Introduction to ionomers. New York: Wiley; 1998.
[56] Zhao W, Zhao X, Rafailovich MH, Sokolov J, Composto RJ, Smith SD, Russell TP, Dozier WD, Mansfield T, Satkowski M. Macromolecules 1993;26:561.
[57] Yoon DY, Vacatello M, Smith GD. Simulation studies of polymer melts at interfaces. In: Binder K, editor. Monte Carlo and molecular dynamics simulations in polymer science. New York: Oxford University Press; 1995. Chapter 8.

[58] Werner A, Schmid F, Muller M, Binder K. J Chem Phys 1997;107: 8175.
[59] Werner A, Schmid F, Muller M, Binder K. Phys Rev E 1999;59:728.
[60] Doruker P, Mattice WL. Macromol Theory Simul 2001;10:363.
[61] Barnes KA, Karim A, Douglas JF, Nakatani AI, Gruell H, Amis EJ. Macromolecules 2000;33:4177.
[62] Toney MF, Mate M, Leach KA. Appl Phys Lett 2000;77:3296.
[63] Chang J, Han J, Yang L, Jaffe RL, Yoon DY. J Chem Phys 2001;115: 2831.
[64] Nijmeijer MJP, Bakker AF, Bruin C, Sikkenk JH. J Chem Phys 1988; 89(6):3789.
[65] Trokhymchuk A, Alejandre J. J Chem Phys 1999;111:8510.